CellPress OPEN ACCESS

Trends in Biotechnology

Research Article

Protein-based molecular imprinting: gelatin nanotraps for interleukin-6 sequestration in inflammation cell models

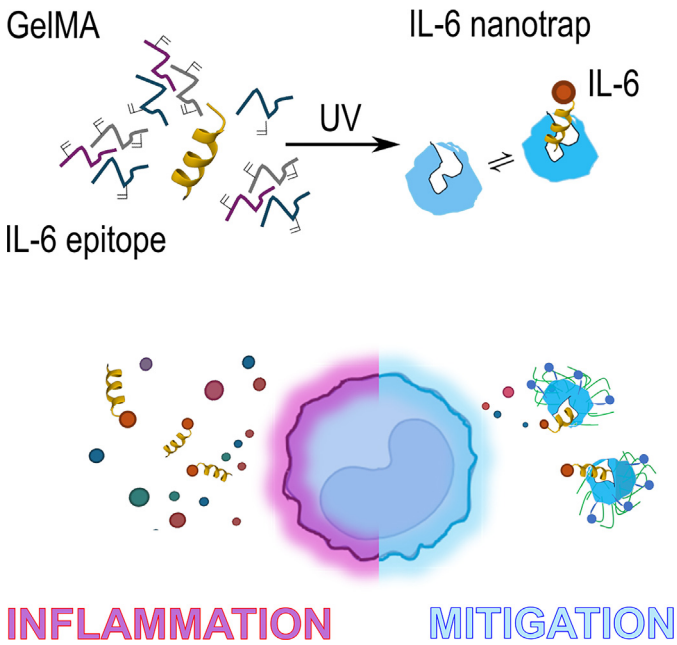

Gelatin methacryloyl (GelMA) was harnessed to create nanotraps via molecular imprinting that were specifically designed to scavenge interleukin-6 (IL-6) in inflammation models. This innovative approach leverages safe and biocompatible protein-based biomaterials, paving the way for a novel class of therapeutic solutions with significant clinical potential.

Alessandra Maria Bossi, Sofia Casella, Chiara Stranieri, Alice Marinangeli, Alessio Bucciarelli, Anna Maria Fratta Pasini, Devid Maniglio

alessandramaria.bossi@univr.it (A.M. Bossi)
devid.maniglio@unitn.it (D. Maniglio).

Highlights

With their inherent biocompatibility and biodegradability, protein-derived biomaterials offer significant untapped potential as building blocks in molecular imprinting.

Gelatin methacryloyl (GelMA) was successfully used to create bioinspired nanotraps designed to target the proinflammatory cytokine interleukin 6 (IL-6).

In vitro, the GelMA nanotraps effectively sequestered IL-6 in an inflammation cell model in a dose–response relationship.

Combining molecular imprinting and protein-derived biomaterials represents a biotechnological innovation to develop functional bio-nanomaterials tailored to suit specific biological applications.

Trends in Biotechnology, Month 2025, Vol. xx, No. xx
https://doi.org/10.1016/j.tibtech.2025.02.002

Trends in Biotechnology

CellPress OPEN ACCESS

Research Article

Protein-based molecular imprinting: gelatin nanotraps for interleukin-6 sequestration in inflammation cell models

Alessandra Maria Bossi [1,*], Sofia Casella [1], Chiara Stranieri [2], Alice Marinangeli [1], Alessio Bucciarelli [3], Anna Maria Fratta Pasini [2], and Devid Maniglio [4,*]

Protein-derived biomaterials are currently underrated as building blocks in molecular imprinting, even though they offer several benefits, such as biocompatibility and safe biodegradability. Gelatin is a biopolymer that can be easily modified with pendant double bonds for polymerization, making it suitable for tissue engineering and biofabrication. In this study, we used gelatin methacryloyl (GelMA) as a building block combined with molecular imprinting technology to create an original class of bioinspired nanotraps specifically capable of sequestering the proinflammatory cytokine interleukin-6 (IL-6). The stability in solution, biocompatibility, and biodegradability of the nanotraps were assessed. The nanotraps were selective and specific for IL-6, showing nanomolar affinity and, when tested *in vitro* on an inflammation cell model, sequestered IL-6 with a dose–response relationship. Overall, our study shows that protein chemistry-driven molecular imprinting could become more widely used to devise biocompatible functional nanomaterials.

Technology readiness

The integration of safe, biocompatible, protein building blocks with molecular imprinting technology to create biomimetic functional nanotraps is currently positioned at Technology Readiness Level (TRL) 3. This proof-of-concept study, using gelatin methacryloyl (GelMA) to fabricate nanotraps for scavenging interleukin (IL)-6, demonstrates potential for advancing inflammation management. Nanotraps could become a promising new class of therapeutics to revolutionize treatment strategies. Progression to TRL4 will require expanding the repertoire of protein-based building blocks and optimizing the synthesis for scalability. Achieving these milestones will set the stage for translational studies, bringing this innovative approach closer to clinical application.

Introduction

Molecularly imprinted polymer (MIP) technology (see Glossary) is a strategy to mold selective binding sites in a material by means of a template-assisted synthesis [1]. Synthesis of MIPs, whether for bulk, thin-films, or **MIP nanoparticles (nanoMIPs)**, is achieved through the use of acrylamides, acrylates, and methacrylate monomers. Notably, acrylamides have emerged as essential components in the fabrication of nanoMIPs [2–4]. Acrylamides are widely used for several reasons, including: the variety of commercially available acrylamide-based monomers, which provide a range of chemical functionalities to optimize the complementarity of the templated binding sites; their aqueous compatibility, allowing the preparation of nanoMIPs in water or in mild solvents; and the physicochemistry of the growing polyacrylamide networks, which leads to nanomaterials with a hydrodynamic size of a few tens to a few hundred nanometers. These features, together with their reported selectivity in biological contexts, laid the foundations for the popularity of polyacrylamide nanoMIPs [3–8].

NanoMIPs have been studied for imaging at cell and tissue levels [9], for *in vivo* removal of toxins [2], to scavenge tumor necrosis factor (TNF)-α from cell supernatants [10], to interfere with metastatic proliferation in cell models [6,11], for protein refolding [12], and even for acting as targeted prodrugs to interrupt cancer cell growth [13]. Despite such uses, the translation of current nanoMIPs to clinical applications is challenging, due to both the limited degradability of the polyacrylamides, which persist *in vivo* for ~8–10 years [14], and the potential toxicity of their degradation byproducts. While widely used in implants as subcutaneous soft tissue fillers, several

[1]Department of Biotechnology, University of Verona, LaStMolCAL Lab, Strada Le Grazie 15, 37134 Verona, Italy
[2]Department of Medicine, University of Verona, A.O.U.I. Verona, Policlinico GB Rossi, P.le L.A. Scuro 10, 37134 Verona, Italy
[3]Laboratorio RAMSES; IRCCS Istituto Ortopedico Rizzoli; Via di Barbiano 1/10, 40136 Bologna, Italy
[4]Department of Industrial Engineering, University of Trento, BIOtech Research Center, Via delle Regole 101, Mattarello, 38123, Trento, Italy

*Correspondence:
alessandramaria.bossi@univr.it (A.M. Bossi) and
devid.maniglio@unitn.it (D. Maniglio).

complications have been reported, in terms of both acute and chronic reactions to polyacrylamide-derived hydrogels, which include inflammatory and granulomatous reactions, which increase in severity following the migration of the injected material to different sites and by its degradation into toxic and immunogenic monomers or oligomers [15–17]. Thus, research has begun to focus on finding more biocompatible solutions for the synthesis of nanoMIPs.

Among the possible solutions, polysaccharides, such as chitosan, have received significant interest [18]. Regardless of whether hydroxyl groups or amines are provided as chemical functionalities, an important question is whether this material forcefully limits the imprinting process to only a few types of interaction. There are few examples of alternative approaches, such as plant oil-based monomers for MIPs [19], or proteins, such as zeins, casein-based MIPs [20], and silk fibroin nanoMIPs [21].

Biotechnology-driven solutions that use proteins as the building blocks to form MIPs and nanoMIPs remain underexplored. Protein physicochemical properties, such as hydrophobicity, sensitivity to temperature and/or pH, can be leveraged to induce controlled, non-native, disordered aggregation, thereby facilitating the formation of smart, functional **bioMIPs** [21,22]. For example, silk fibroin, a protein with high biocompatibility and already in use in tissue engineering, as well as with a propensity to fold into beta-structures [23], was exploited to nucleate and rigidize bioMIPs. Widening the portfolio of biocompatible, bioderived building blocks for bioMIP synthesis by expanding research on protein-based building blocks seeks to capitalize on natural evolution, which has resulted in numerous proteins for manifold purposes, and forms the basis for an innovative biotech-strategy for the development of bioMIPs.

There are several key advantages to exploiting protein-based building blocks: (i) proteins have significant variability in their amino acid sequences, providing charged, hydrophobic, and hydrophilic functionalities suitable for the molecular recognition of the intended target molecule; (ii) the propensity of protein sequences to form secondary and tertiary structures, and even superstructures [24], can be exploited to drive nucleation and ultimately govern the size of bioMIPs; (iii) each protein has specific functionalities (e.g., biorecognition motifs and typical degradation times) that can be exploited in bioMIPs to elicit specific behaviors when required, such as fine-tuning the targeting of biomolecules or tailoring their half-life.

Gelatin, obtained by the denaturation and fragmentation of collagen [25], shows particular promise among proteins able to form superstructures. Currently, it is used in tissue engineering and regenerative medicine, specifically in wound dressings, given its ability to promote cell adhesion and proliferation, together with its excellent biocompatibility, nontoxicity, and nonimmunogenicity [26,27]. Gelatin can be functionalized with pendant double bonds by **methacrylation** (forming **GelMA**) [25], highlighting its potential to undergo radical polymerization processes and crosslinking [28].

Here, we report the design of bioinspired molecular **nanotraps** in the form of functional disordered protein superassemblies based on the molecular imprinting of gelatin-derived building blocks. The GelMA bioMIP nanotraps were rendered selective for IL-6 by using an **epitope imprinting strategy** [29,30] and choosing a specific solvent-exposed IL-6 peptide segment as the **epitope**.

IL-6 is a multifunctional cytokine with a key regulatory role in inflammation [31,32]. It is secreted by various immune cells, such as macrophages, dendritic cells, and T cells, in response to pathogens or tissue damage [31–35]. Elevated levels of IL-6 occur in severe conditions, such as sepsis, and are implicated in the transition from acute to chronic inflammation. Monitoring IL-6 levels helps evaluate the severity of the inflammation and can be prognostic of the response to

Glossary

BioMIPs: general term to refer to MIPs prepared using naturally derived materials as the starting material, such as proteins (GelMA or silk fibroin), polymerized to form bioinspired functional protein aggregates.
Epitope: specific and recognizable fragment of a larger target molecule, such as a peptide segment of a protein, used as the template during the imprinting process.
Epitope imprinting strategy: imprinting process when using an epitope as a template; used to form MIPs with high specificity for the larger target by mimicking the natural interaction with the selected epitope.
Gelatin: natural biopolymer derived from the partial hydrolysis of collagen, typically obtained from animal connective tissues, such as skin, bones, and cartilage; comprised primarily of glycine, proline, and hydroxyproline amino acids, arranged in a random-coil structure. It is widely used in biotechnology, medicine, and food industries due to its biocompatibility, biodegradability, and ability to form hydrogels. It can be chemically modified, for example, through methacrylation, to enhance its functionality for applications in tissue engineering, drug delivery, and molecular imprinting.
Gelatin methacryloyl (GelMA): fragmented gelatin to which polymerizable double bonds have been added; it is the building block of the nanotraps.
Gelatin methacryloyl nanoparticles (GelMA NPs): GelMA polymerized in the form of NPs.
Molecular imprinting technology: process of molding molecular recognition sites in materials using template-assisted synthesis.
Molecularly imprinted polymeric nanoparticles (MIP NPs/nanoMIPs): prepared from acrylamides, acrylates, and methacrylates; often referred to as plastic antibodies.
Nanotraps: GelMA polymerized using a molecular imprinting approach in the presence of a template, such as the specific IL-6 C terminus epitope used here. The resulting nanotraps are protein-disordered aggregates of nanometric size that exhibit specific and selective recognition for their targeted molecule (in this case IL-6).

treatment. The extent to which modulating IL-6 levels contributes to mitigating inflammation is under assessment [36,37]. To date, strategies leveraged to counteract inflammation include monoclonal antibodies (MAbs) used to clinically target IL-6 signaling [38]. Despite MAbs being well tolerated, adverse events have been observed in long-term clinical trials. Alternatives include engineered proteins, such as Alphabodies [39] or Repebodies [40,41], or chemically synthesized telodendrimer (TD) nanotraps, which have been reported to show immune modulation [42,43]. Despite such strategies, a solution to mitigate inflammation is far from being achieved. Thus, devising a strategy to form nanotraps comprising an intrinsically safe material and that are IL-6 selective could represent an additional tool for future therapies. Such aqueous-soluble nanotraps prepared with GelMA and stabilized by photocrosslinking could behave as biomimetic receptors that are effective in sequestering IL-6, at least up to the level of cellular models of inflammation.

Results

Conditions required to form GelMA nanoparticles

The conditions required to prepare homogeneous populations of **GelMA NPs** from GelMA building blocks were determined by combining experimental data and the Response Surface Method (RSM) model (Figure 1; SI 2,3 in the supplemental information online) [44]. Transferring the state-of-the-art conditions for the preparation of plastic antibodies [2,9,45], GelMA NPs were synthesized with highly diluted GelMA building-blocks to support the in-solution 'nucleation' of individual GelMA NPs, while keeping them statistically far apart from one another to avoid coalescence (Figure 1A). Next, photocrosslinking by means of the biocompatible photoinitiator lithium phenyl-2,4,6-trimethyl benzoylphosphinate (LAP) [46] was used to fix the discrete GelMA superassemblies into single NPs. Homogeneous GelMA NPs with a polydispersity index (PDI) ≤0.3 and an average diameter of 70–110 nm (Figure 1B–D) were obtained in pH conditions ranging from 5.5 to 8.3. The set synthetic conditions were 0.3% w/v GelMA in phosphate buffer saline (PBS) at pH 7.4 and 0.02% w/v LAP. Atomic force microscopy (Figure 1E) and scanning electron

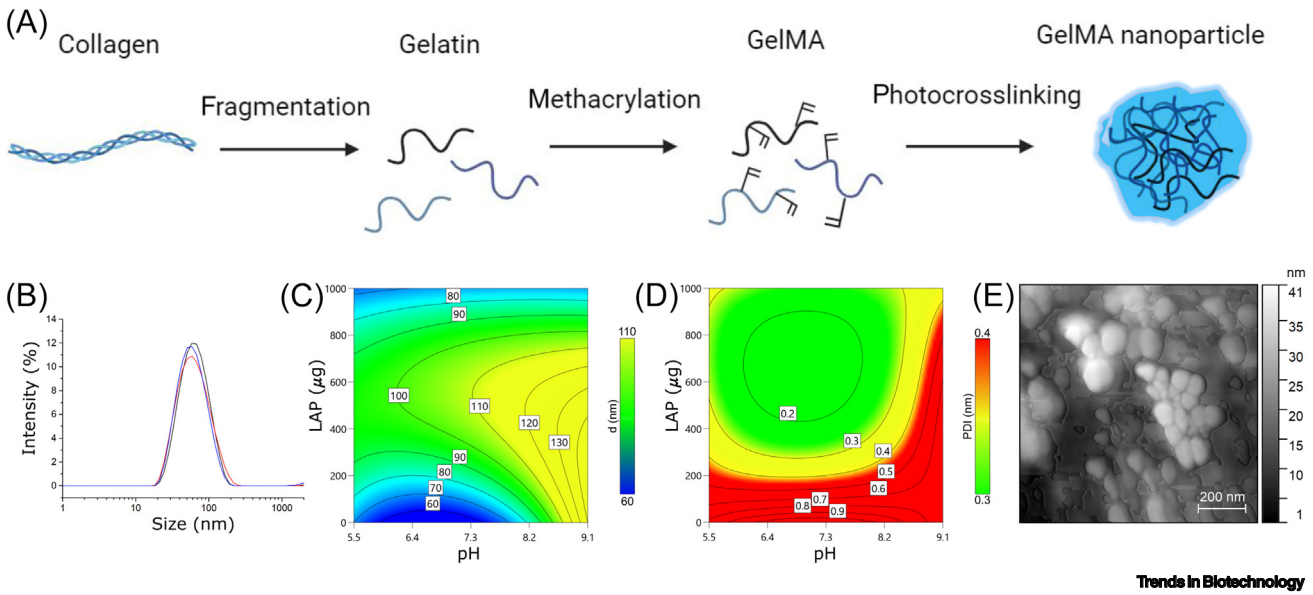

Figure 1. Condition required to form GelMA nanoparticles. (A) General route for gelatin methacryloyl nanoparticle (GelMA NP) preparation. (B) Hydrodynamic diameter of GelMA NPs. (C) Size distribution of GelMA NPs determined by the Response Surface Method using the following input parameters: concentration of the GelMA building blocks (2.6, 1, 0.3, or 0.03 % w/v), the pH of the aqueous solvating buffer (pH 5.5, 7.4, or 9.1), and the amount of photo-initiator, while output parameters were the size and (D) polydispersity index (PDI) of the GelMA NPs. (E) Atomic force microscopy image of the GelMA NPs. Abbreviation: LAP, lithium phenyl-2,4,6-trimethylbenzoylphosphinate.

microscopy (SI 18 in the supplemental information online) were used to assess the resulting GelMA NPs.

The mean molecular weight (MW) of the GelMA NPs, estimated by static light scattering (SLS; SI 4 in the supplemental information online), was 2.50 ± 0.15 MDa. A more accurate MW of the GelMA NPs was calculated using Equation 1 [47]:

$$M_{GelMA\ NPs} = 4/3\pi R^3 \rho N_A \quad [1],$$

where R is the radius of GelMA NPs when collapsed, so to exclude the volume of the NP occupied by the hydration water (R = 20 nm, details in SI 21 in the supplemental information online), ρ is the density of gelatin (0.72 g/cm^3), and N_A is Avogadro's number. This resulted in a MW of 1.45 MDa, which was the same order of magnitude as that achieved with SLS, but more accurate given the correction for hydration; thus, this value was used in further experiments.

GelMA NPs were stable in solution for up to 96 h (PDI <0.3; Figure 2A,B). To further extend the in-solution stability and, ultimately, their shelf-life, linear short-chains of polyethylene glycol (PEG)-methacrylate (PEGMA; M_n 500 Da) [48] were coupled to the GelMA NPs. Camouflage by PEG decoration was explored in solutions of PEGMA:GelMA NPs with molar ratios ranging from 1:2 to 500:1; this was confirmed with NMR based on a clear signal at 3.60 ppm corresponding to

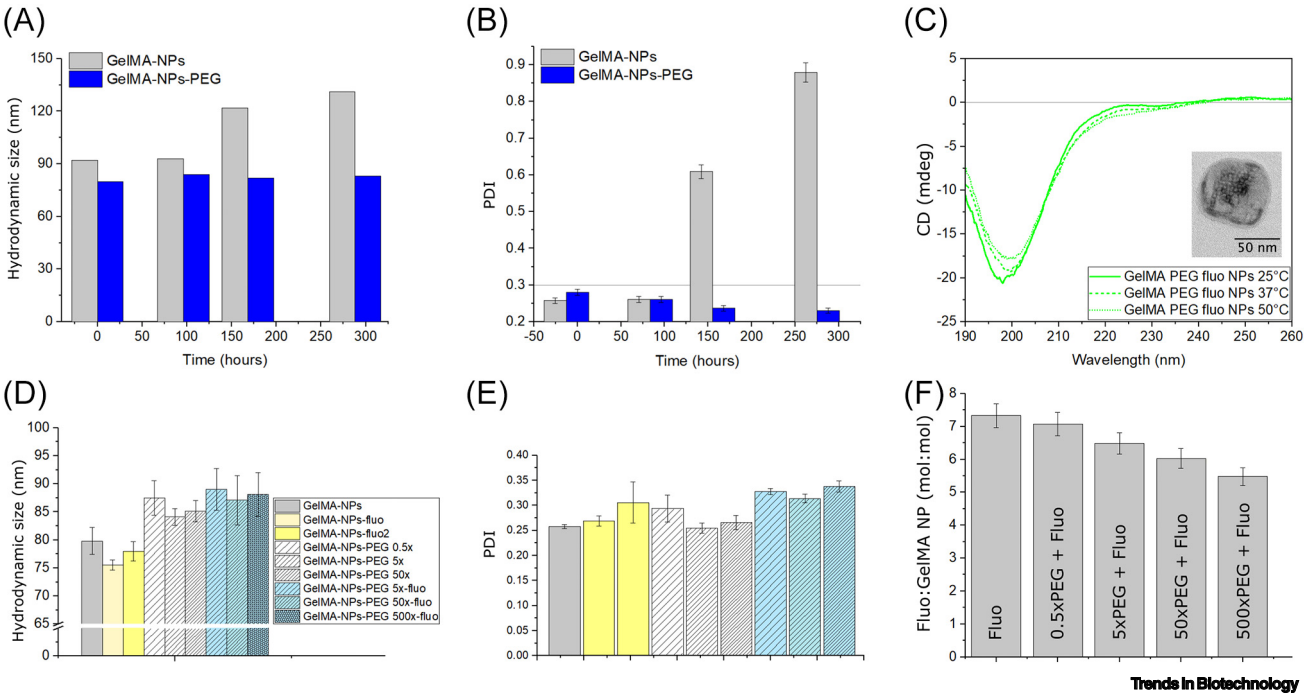

Figure 2. Physical characterization of gelatin methacryloyl nanoparticles (GelMA NPs). Stability over time of GelMA NPs (gray bars) and polyethylene glycol (PEG)-camouflaged GelMA NPs (blue bars) investigated as (A) changes in hydrodynamic size over time and (B) the polydispersity index (PDI), showing that PEG camouflage significantly improved the stability of the NPs. (C) Circular dichroism (CD) of the GelMA NPs confirmed the absence of secondary structures in the protein superassemblies, suggesting instead disordered protein NPs. Inset: representative transmission electron microscope (TEM) image of a GelMA-PEG NP. (D) Hydrodynamic size and (E) PDI of GelMA NPs. Solid gray, GelMA NPs; solid yellow, fluorescently labeled GelMA NPs (fluo: Rhodamine; fluo2: Nile Blue); stripes of increasing density, GelMA NPs camouflaged with increasing PEG (0.5×; 5×; 50×; and 500×); light-blue bars with stripes, GelMA NPs PEG camouflaged and fluorescently labeled. (F) Incorporation of fluorescent labels as a function of the amount of PEG methacrylate (PEGMA) used for the camouflage: bars represent the estimated moles of fluorescent labels incorporated per mol of GelMA NPs, for camouflage performed at increasing PEG concentrations (0.5×, 5×, 50×, and 500×). Data are mean ± standard deviation.

-OCH2- groups in the NMR spectrum (SI 5 in the supplemental information online). PEGylation, which was estimated as 0.38 mol% of the GelMA when 500× PEG was used, did not significantly alter the zeta-potential (SI 20 in the supplemental information online) or the hydrodynamic sizes and PDIs of the GelMA NPs (Figure 2D,E and SI 6 in the supplemental information online), but did prolong the in-solution stability for up to 288 h (Figure 2A,B, blue bars).

The decoration of GelMA NPs with fluorescent labels was then considered for imaging purposes. The photocoupling of either acryloxyethyl thiocarbamoyl Rhodamine B, or Nile Blue acrylamide to GelMA NPs, confirmed by fluorescence spectroscopy (SI 17 in the supplemental information online), did not significantly alter the hydrodynamic size or the PDI compared with bare GelMA NPs (Figure 2D,E). The incorporation of the fluorescent dye on the GelMA NPs was inversely correlated to the concentration of PEGMA used for camouflage (Figure 2F). Finally, the structural characteristics of GelMA NPs, investigated by circular dichroism (CD) (Figure 2C), showed disordered superassemblies of GelMA both above and below the gelation temperature (36°C; SI 7 in the supplemental information online).

IL-6 GelMA nanotraps

GelMA nanotraps specific for the recognition of IL-6 were prepared by using an epitope imprinting strategy [29]. The 3D structure of IL-6 (UniProtKB P05231) was examined (Figure 3) using bioinformatics tools to identify a unique and accessible peptide suitable as a template for the imprinting process, following the method of Pasquardini and Bossi [30]. The 13mer of sequence EFLQSSLRALRQM, which corresponds to the IL-6 C terminus, was idiotypic for IL-6 (SI 8 in the supplemental information online) [49]. The Peptide Atlas (query PAp00506237), which is a curated repository of clinically reported immuno-targeted sequences, confirmed the uniqueness of the EFLQSSLR sequence for IL-6 in the proteome, as also shown experimentally [50,51]. Furthermore, PEP-FOLD3 [52], used to predict the conformation of the chosen epitope, predicted the helix motif of IL-6 (SI 9 in the supplemental information online).

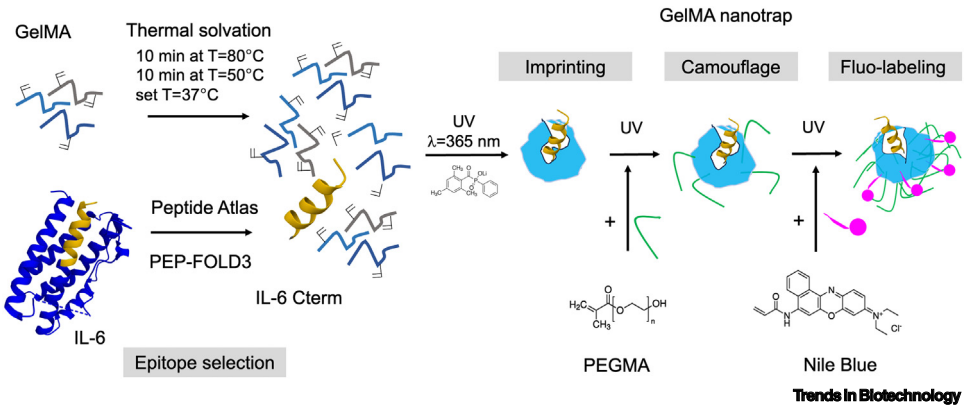

Figure 3. Schematic of the preparation of interleukin (IL)-6 gelatin methacryloyl (GelMA) nanotraps. The solvent-accessible 13mer, EFLQSSLRALRQM, which corresponded to the IL-6 C terminus (IL6Cterm), was idiotypic for IL-6 and was used thereafter as the epitope template during the imprinting process. Following thermal dissolution of GelMA in phosphate buffer saline (PBS), the temperature was maintained at 37°C for the whole process. The epitope-template IL-6Cterm was solvated with GelMA under conditions previously reported to yield protein superassemblies. The system was allowed to equilibrate, and the photocrosslinker lithium phenyl-2,4,6-trimethylbenzoylphosphinate (LAP) was added. The radical photopolymerization of the unsaturated C=C double bonds was triggered by UV light. Ensuing steps were the coupling of polyethylene glycol methacrylate (PEGMA), to provide camouflage to the IL-6 nanotraps, and labeling with a polymerizable fluorophore (Nile Blue or Rhodamine). At the end of the process, the nanotraps were extensively washed to remove the epitope template, freeing the stamped molecular sites to bind IL-6 (only one shown here for simplification).

For imprinting, GelMA (3 mg/ml) was thermally dissolved using conditions previously optimized for preparing GelMA NPs, and IL-6Cterm (6 nmol) was added to the solution. It was hypothesized that the lateral groups of the amino acids comprising GelMA provide a variety of chemical functionalities to interact with IL-6Cterm. Thus, the resulting molecular pairing was assumed to drive the imprinting process, ultimately leading to the formation of the templated binding sites. The photopolymerization of the GelMA pendant double bonds stabilized the GelMA superassemblies and fixed the stereochemistry of the imprinted binding site.

The resulting imprinted nanotraps were then camouflaged and fluorescently tagged and, finally, the template was removed by a thermal wash (SI 10 in the supplemental information online). Figure 4 details the physical and functional characteristics of the nanotraps (SI 11 in the supplemental information online). Their average hydrodynamic size (Figure 4A) was 86–92 nm with PDIs ≤0.24 (Figure 4B), indicating a homogenous population. CD (Figure 4C) confirmed that the structure was a random coil, showing that the nanotraps were disordered superassemblies of GelMA units, similar to that observed for GelMA NPs.

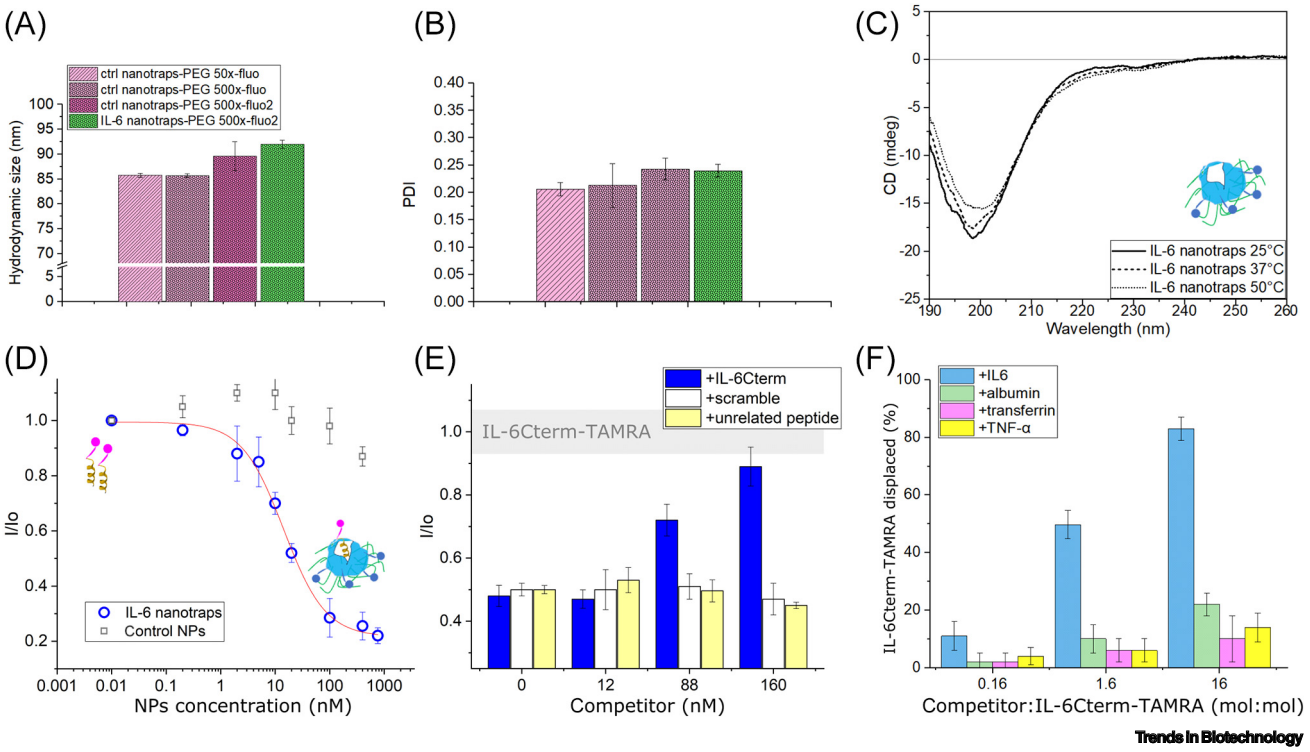

Figure 4. Characterization of the interleukin (IL)-6 nanotraps. (A) Hydrodynamic size and (B) polydispersity index (PDI) of nanotraps: control nanotraps were prepared with a template peptide nonrelated to IL-6 and camouflaged with polyethylene glycol (PEG) 50× (light pink, light stippling), or with PEG 500× (light pink, dense stippling), or with PEG 500× and fluorescent label (fluo: Rhodamine, light pink; fluo2: Nile Blue, dark pink). Green bar represents IL-6 nanotraps, camouflaged with PEG (500×) and labeled with Nile Blue. (C) Circular dichroism (CD) of IL-6 nanotraps confirmed the absence of secondary structures, suggesting instead disordered protein superassemblies, similar to the non-imprinted gelatin methacryloyl nanoparticles (GelMA NPs) (see Figure 2C in the main text). (D) Binding isotherm of IL-6 nanotraps to IL-6 C terminus (IL6Cterm)-TAMRA: blue circles represent experimental values (n = 3); red line represents nonlinear fitting; gray squares represent non-imprinted GelMA NPs (controls). (E) Selectivity test with peptides. Competition between IL-6Cterm-TAMRA (47.5 nM) and increasing concentrations of IL-6Cterm (blue bars) scrambled IL-6Cterm of sequence FLQERSSLRQMAL (clear bars) or AYATEPHAK peptide from cardiac troponin I, nonrelated to IL-6 (yellow bars), for binding to the IL-6 nanotraps (12.5 nM). (F) Selectivity test with proteins. The competitive conditions used were: 0.16, 1.6, and 16 competitor:IL-6Cterm-TAMRA moles ratios. The bound IL-6Cterm-TAMRA was challenged with increasing concentrations of: IL-6 (light-blue bars), serum albumin (green bars), serum transferrin (pink bars), or tumor necrosis factor (TNF)-α (yellow bars). Data are mean ± standard deviation.

The expected imprinting effect on the nanotraps was assessed by testing their ability to specifically rebind the IL-6Cterm template peptide. A fluorescently labeled IL-6Cterm [i.e., IL-6Cterm-TAMRA (250 nM), SI 16 in the supplemental information online] was incubated in the presence of increasing nanotrap concentrations (0.01–760 nM) (Figure 4D). Quenching of the IL-6Cterm-TAMRA fluorescence emission was observed upon nanotrap binding [53,54]. While control GelMA NPs showed no binding (Figure 4D, gray squares), a typical saturation curve with a characteristic sigmoidal profile was reported for nanotrap binding, supporting the presence of a defined number of binding sites and accounting for effective imprinting (Figure 4D, blue circles). The nonlinear fitting of the experimental data enabled estimation of a nanomolar apparent dissociation constant (K_{Dapp} 16.31 ± 1.84 nM) with no cooperativity (n = 1.06 ± 0.18) (SI 12 in the supplemental information online). The number (N) of binding sites for IL-6Cterm and for IL-6 on each NP was calculated using Equation 2 [47]:

$$N = \frac{\frac{4}{3}\pi R^3 \rho Q_{max} N_A}{M} \quad [2],$$

where R is the radius of a single nanotrap, shrunk to exclude the water contained within the GelMA hydrogel network ($R \approx 20$ nm); Qmax is the saturated adsorption amount of IL-6Cterm or of IL-6 bound by nanotraps per nanotrap weight (g); ρ is the density of hydrated gelatin (0.72 g/cm^3); N_A was 6.022 × 10^{23} mol^{-1}, $M_{IL\text{-}6Cterm}$ = 1577.84 Da, and $M_{IL\text{-}6}$ = 20 900 Da. The estimated number of binding sites per nanotrap was $N \approx 4$ for IL-6Cterm, and $N \approx 6$ for complete IL-6. Given the heuristic nature of the input parameters, these N values can be considered similar and support the formation of a low number of binding sites per nanotrap.

The selectivity of the nanotraps for IL-6Cterm was proven by competition experiments. Figure 4E shows that IL-6Cterm (blue bars) displaces the IL-6Cterm-TAMRA bound to nanotraps, indicating that it is an effective competitor. By contrast, when the competitor was the scrambled sequence of the IL-6Cterm peptide, it did not produce a displacing effect (Figure 4E, clear bars). Similarly, no displacement was observed when the competitor was a peptide nonrelated to IL-6 (Figure 4E, yellow bars). These results proved the selectivity of the nanotraps and confirmed a sequence-related ability to discriminate the target, showing that molecular imprinting had occurred.

Next, selectivity was tested at the whole-protein level. IL-6 promoted a marked displacement of IL-6Cterm-TAMRA, indicating the binding of the whole cytokine (Figure 4F). By contrast, when tested with another cytokine (TNF-α), no significant displacement was reported. Likewise, limited to no displacement was observed for the serum proteins albumin and transferrin, which were used as controls for nonspecific binding. These experiments confirmed the selectivity of the nanotraps at the protein level. Finally, the binding behavior of the IL-6 nanotraps was thermodynamically validated by isothermal titration calorimetry (ITC) (SI 13 in the supplemental information online). Overall, the results affirmed the nanomolar affinity of the nanotraps and their selectivity for IL-6.

Nanotrap storage, reconstitution, and enzymatic degradation

The storage, handling, and degradation of the IL-6 nanotraps were also investigated. Nanotraps (3 mg/ml) were freeze-dried and stored at –20°C for up to 6 months. Before use, samples were rehydrated for 3 h, analyzed using dynamic light scattering (DLS), and compared with freshly synthesized nanotraps (SI 14 in the supplemental information online). The Z-average was 85.1 ± 1.9 nm (PDI = 0.266 ± 0.011) and 93.3 ± 0.2 nm (PDI = 0.274 ± 0.008) for fresh and reconstituted samples, respectively. These results showed the complete rehydration of the samples, while low PDIs ensued their colloidal stability, showing that it is possible to freeze-dry these nanotraps for storage.

When considering the possible therapeutic uses of nanotraps, their *in vivo* fate needs to be ascertained. Thus, nanotraps were subjected to enzymatic degradation by using either trypsin or proteinase K [40] overnight at 37°C and results were monitored using DLS (SI 15 in the supplemental information online). A reduction in the Z-average was observed with a concomitant increase in PDIs (up to PDI = 1), supporting the biodegradation of the nanotraps and suggesting biological pathways for their *in vivo* clearance.

IL-6 nanotraps sequester IL-6 in a cell inflammatory model

The final objective of this work was to investigate whether the nanotraps could be used to modulate the immune response by trapping IL-6 released during inflammation (Figure 5A). To do so, the human leukemic monocyte THP-1 cell line was used for immunomodulation experiments [55]. First, the biocompatibility of the nanotraps with THP-1 cells was assessed with the AlamarBlue® test over an 8-day period, which showed that the cells remained fully viable (SI 19 in the supplemental information online). The viability of differentiated THP-1 cells exposed to the nanotraps was also investigated by fluorescence-activated cell sorting (FACS). Nanotraps (1.67 mg/ml)

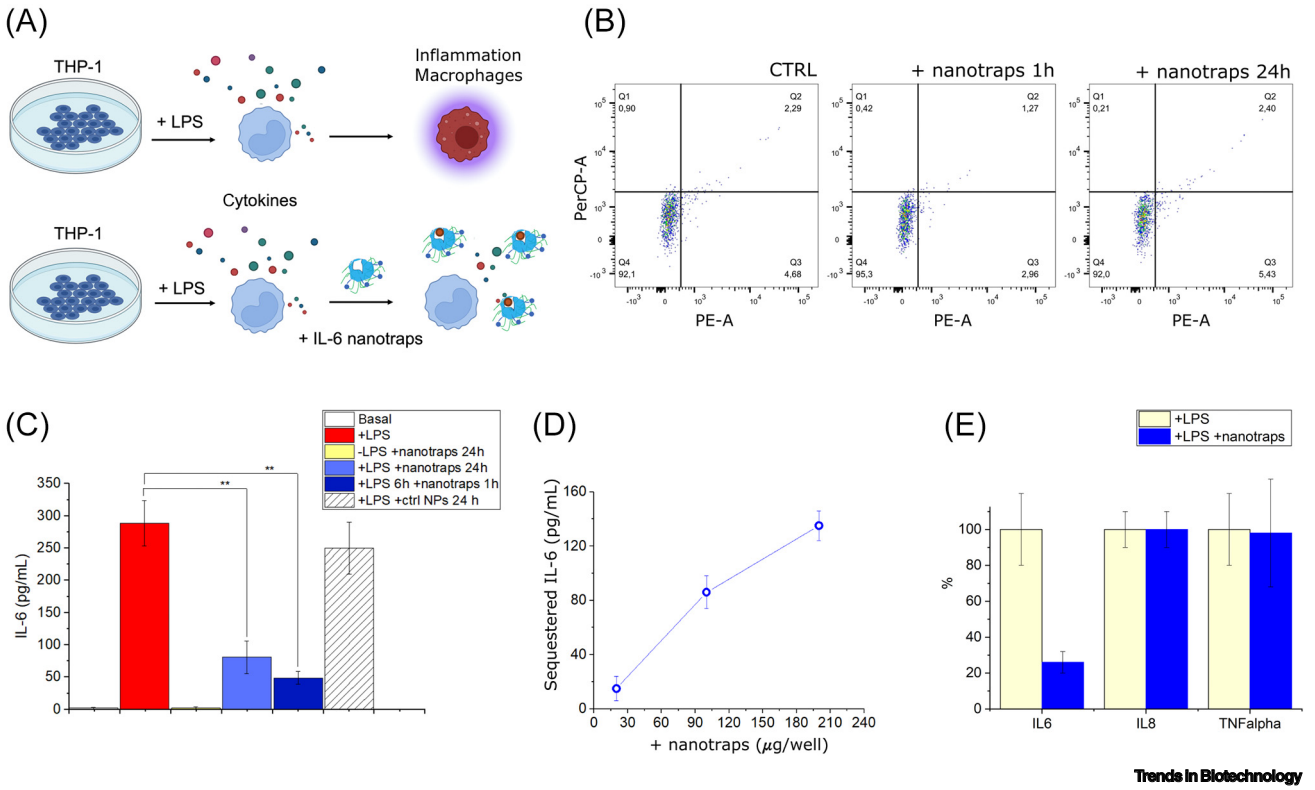

Figure 5. Test of the ability of IL-6 nanotraps to sequester IL-6 in a inflammatoty cell model. (A) Scavenging effect of nanotraps on the proinflammatory molecule interleukin (IL)-6. (B) Flow cytofluorimetry of control THP-1 cells (ctrl) compared with THP-1 cells + nanotraps (1.67 mg/ml) after 1 h or 24 h showed that the presence of nanotraps in the cell culture did not stimulate pre-apoptosis or apoptosis. (C) Trapping of IL-6 from differentiated THP-1 cells: THP-1 stimulated with lipopolysaccharide (LPS) (1 μg/ml) showed production of IL-6 (244 ± 67 pg/ml; red bar); when THP-1 cells were simultaneously treated for 24 h with both LPS and nanotraps (150 μg) the concentration of IL-6 decreased to 52 ± 29 pg/ml (light-blue bar); when THP-1 were stimulated with LPS (1 μg/ml) for 6 h and then incubated for 1 h with the nanotraps (150 μg), the level of IL-6 decreased to 46 ± 26 pg/ml, confirming the scavenging effect of the nanotraps and a reduction in IL-6 of ~81% (blue bar). As a control, differentiated THP-1 cells before stimulation showed a basal level of IL-6 of 0.51 pg/ml (white bar); IL-6 was not detected in THP-1 cells incubated in the presence of nanotraps alone (yellow bar), and neither did control non-imprinted GelMA NPs show significative uptake of IL-6 (striped white bar). (D) Dose–response relationship of nanotraps on the level of IL-6 in the supernatants of differentiated THP-1 cells stimulated with LPS (n = 4). (E) Selectivity of the nanotraps versus cytokine uptake. The levels of IL-6, IL-8 and tumor necrosis factor (TNF)-α were tested after both the addition of LPS (yellow bars) and 24 h of treatment with nanotraps (blue bars). Results suggested that the nanotraps selectively removed IL-6 from the cell cultures (n = 3). Data are mean ± standard deviation; One-way ANOVA with post-hoc Tukey HSD (Honestly Significant Difference), $^{**}P < 0.01$.

were co-incubated with THP-1 cells (5×10^5 cells/well, V = 250 µl) for up to 24 h. The percentage of viable cells (Q4) remained constant under all conditions and at all time points (i.e., ctrl 92.1%; + nanotraps 1 h 95.3%; + nanotraps 24 h 92.0%), with non-significant percentages of pre-apoptotic (Q1) or apoptotic (Q2) cells (Figure 5B). Furthermore, no nanotrap uptake by THP-1 cells was observed (SI 22 in the supplemental information online). These results fully supported the biocompatibility of the nanotraps, highlighting their potential therapeutic use to modulate inflammation.

To investigate this further, differentiated THP-1 cells were treated with lipopolysaccharide (LPS) [56,57] to induce an inflammatory response eliciting the expression of IL-6. LPS induces the release of IL-6 in the supernatant, with a maximum reached 6 h after exposure [56]. In our experiment, LPS stimulation (24 h) increased the IL-6 level in the differentiated THP-1 culture to 244 ± 67 pg/ml (Figure 5C, red bar). Control THP-1 cells did not produce IL-6 in the absence of LPS (0.51 pg/ml; Figure 5C; basal, clear bar) and neither did THP-1 cells cycled for 24 h in the presence of nanotraps alone (0.28 pg/ml; Figure 5C, yellow bar), further confirming that the nanotraps did not trigger an inflammatory response. Differentiated THP-1 cells simultaneously treated for 24 h with both LPS and nanotraps (150 µg) showed a 79% reduction in IL-6 (Figure 5C, light-blue bar), indicating the sequestering effect of the nanotraps.

To exclude the nonselective effects of the nanotraps on LPS, THP-1 cells were treated with LPS for 6 h to maximize IL-6 release; nanotraps (150 µg) were then added to the culture for 1 h. There was an 81% reduction in IL-6 in treated versus with nontreated cells, demonstrating the selective sequestering of IL-6 from the cell medium by the nanotraps (Figure 5C, blue bar). Addition of control GelMA NPs (Figure 5C, white-striped bar) did not result in a marked uptake of IL-6.

Furthermore, the removal of IL-6 was studied as a function of the concentration of nanotraps used. Nanotraps (20, 100, and 200 µg) were added to LPS-stimulated THP-1 cultures (Figure 5D), resulting in dose–response sequestering of IL-6. Finally, the selectivity of the nanotraps for IL-6 was confirmed by comparing the levels of IL-6 with those of other cytokines (IL-8 and TNF-α) in LPS-stimulated THP-1 cells treated or not with the nanotraps for 24 h. Only IL-6 underwent a significant reduction, indicating the IL-6 specificity of these nanotraps (Figure 5E).

Discussion

Here, we demonstrated the design of molecularly imprinted structurally disordered protein superassemblies as a new class of nano-biomimetics capable of targeting biological signaling molecules. The biocompatible polymer GelMA was molecularly imprinted to specifically recognize the proinflammatory cytokine IL-6. The resulting gelatin-based IL-6 nanotraps were nanometric in size (~80 nm), were camouflaged by short PEG chains for effective biointerfacing [58], and were fluorescently tagged to allow imaging. Camouflaged nanotraps were stable for >10 days in suspension and for >6 months when freeze-dried, allowing their long-term storage. The nanotraps proved selective and specific for IL-6, demonstrating a nanomolar affinity for their target. *In vitro*, the nanotraps removed IL-6 directly from differentiated THP-1 cell cultures previously exposed to LPS to stimulate inflammation. These results suggest that the nanotraps are able to intervene in the inflammatory path via a similar mechanism of action to that used by clinically tested MAbs and other intended therapeutics of biomimetic origin [37–42], including of MIP-based nanozymes designed to bind and inactivate IL-6 [59]. The effective removal of IL-6 from the cell culture medium suggests the successful design of specific and selective molecular traps.

We showed for the first time that GelMA can be used for preparing functionally imprinted nanotraps, thus suggesting the general use of proteins as building blocks for molecularly

imprinted biomimetics starting from natural origin biomaterials, including silk fibroin and gelatin, but also expanding the portfolio to other biomaterials. Using different protein-building blocks to form the bioMIPs could lead to nanotraps characterized by markedly different time-dependent degradation; for example, gelatin displays a much shorter (days to weeks) degradation time compared with silk (weeks to months). Thus, the composition of functional bioMIPs could be tailored to suit the specific biological application, therefore expanding the clinical use of this imprinting technology [60]. Combining this technology with biopolymers could be a game-changing strategy to form therapeutic, safe, biocompatible, and biodegradable molecular traps appropriate for *in vivo* translation. The characteristic disordered protein superassemblies that comprise nanotraps that do not fold but have selective molecular recognition functions could positively impact the scalability of the technology, making it more affordable compared with antibodies. Overall, the combination of GelMA with MIP technology contributes to reinforcing and expanding the concept of protein chemistry-driven molecular imprinting, highlighting the future therapeutic potential of such an approach.

Concluding remarks

The present study pioneers the use of GelMA to develop biomimetic nanotraps through molecular imprinting that are specifically designed to scavenge IL-6 in inflammation models. This advance introduces a groundbreaking approach to molecular imprinting by leveraging safe and biocompatible protein-based biomaterials, paving the way for the development of a new class of therapeutics.

Protein-based nanotrap technology is poised for expansion and scalability. By using a variety of safe protein building blocks, each with distinct degradation profiles, it becomes possible to design nanotraps tailored to specific biological applications. These functional NPs represent a significant step toward creating therapeutic, biodegradable, and biocompatible molecular traps that are safer, more scalable, and more cost-effective compared with mAbs, with significant promise for clinical translation (see Outstanding questions).

Outstanding questions

Can molecular imprinting be applied to other natural proteins to expand the portfolio of bioMIP nanotraps with tailored degradation rates and functional properties?

What are the *in vivo* efficacy and safety profiles of GelMA-based nanotraps in preclinical animal models?

How can the synthesis of bioMIP nanotraps be scaled and optimized to ensure affordability and feasibility for clinical applications? Does solid-phase synthesis represent a feasible solution?

Which computational approaches can be developed to model the pairing of unfolded protein chains with template peptides for the *in silico* design of bioMIPs?

Which additional signaling molecules or pathological biomarkers could benefit from targeted bioMIP nanotraps, and how might this influence therapeutic innovation?

How do bioMIP nanotraps perform in terms of stability, specificity, and functionality compared with antibody-based therapies in real-world clinical settings?

STAR★METHODS

Detailed methods are provided in the online version of this paper and include the following:

- KEY RESOURCES TABLE
- EXPERIMENTAL MODEL AND STUDY PARTICIPANT DETAILS
- METHOD DETAILS
  - GelMA preparation
  - Synthesis of GelMA NPs
  - Synthesis of IL-6 GelMA nanotraps
  - Effect of the lyophilization on GelMA NPs
  - Effect of camouflage on the stability of the GelMA NPs
  - Effect of camouflage with PEGMA
  - Response surface method
  - Atomic force microscopy (AFM)
  - Electron microscopy
  - Dynamic light scattering (DLS)
  - Static light scattering (SLS)
  - Yield of the synthesis
  - Circular dichroism (CD)
  - Binding isotherm of IL-6 nanotraps
  - Competition experiments
  - Cell culture
  - Cell proliferation and metabolism
  - Cell viability
  - Uptake of nanotraps by THP1 cells

- Effect of nanotraps on the IL-6 levels in the cell inflammatory model
- Dose–response relationship

Resource availability

Lead contact

Further information and request for resources and reagents should be directed to and will be fulfilled by the lead contact Alessandra Maria Bossi (alessandramaria.bossi@univr.it).

Materials availability

Reagents are available upon request with a material transfer agreement (MTA).

Data code and availability

No original code was generated with this work.

Acknowledgments

NMR experiments and data analysis were kindly performed by Emanuela Callone using equipment from the 'Klaus Müller' NMR Laboratory of the Industrial Engineering Department at the University of Trento. A.M.B. thanks Centro Piattaforme Tecnologiche (CPT) of the University of Verona for use of their nanoITC, DLS, and Zetasizer facilities. A.B. was supported by IRCCS Istituto Ortopedico Rizzoli (Ricerca Corrente). The present research was carried out within the European Union – NextGenerationEU, component M4C2, investment 1.1, project PRIN2022 'nanoTRiCKS': tailor-made biopolymeric nanotraps for cytokines' storm suppression, project code 20228AYRJE, codes: CUP B53D23008610006 for A.M.B. and CUP E53D23005160006 for D.M. and project PRIN2022 PNRR 'BIAS': Biomips ImmunomodulAting Scaffolds for tissue engineering', project code P2022HLS3M, codes: CUP E53D23017730001 for D.M. and CUP B53D23027570001 for A.M.B. Parts of the figures were created with BioRender (biorender.com).

Declaration of interests

The authors declare no competing interests.

Supplemental information

Supplemental information to this article can be found online at https://doi.org/10.1016/j.tibtech.2025.02.002.

References

1. Arshady, R. and Mosbach, K. (1981) Synthesis of substrate-selective polymers by host-guest polymerization. *Die Makromol. Chem.* 182, 687–692
2. Hoshino, Y. *et al.* (2008) Peptide imprinted polymer nanoparticles: a plastic antibody. *J. Am. Chem. Soc.* 130, 15242–15243
3. Piletsky, S. *et al.* (2020) Molecularly imprinted polymers for cell recognition. *Trends Biotechnol.* 38, 368–387
4. Canfarotta, F. *et al.* (2016) Solid-phase synthesis of molecularly imprinted nanoparticles. *Nat. Protoc.* 11, 443–455
5. Xu, J. *et al.* (2017) Guide to the preparation of molecularly imprinted polymer nanoparticles for protein recognition by solid-phase synthesis. *Methods Enzymol.* 590, 115–141
6. Rangel, P.X.M. *et al.* (2020) Chemical antibody mimics inhibit cadherin-mediated cell–cell adhesion: a promising strategy for cancer therapy. *Angew. Chem. Int. Ed.* 59, 2816–2822
7. Bossi, A.M. (2020) Plastic antibodies for cancer therapy? *Nat. Chem.* 12, 111–112
8. Ding, F. *et al.* (2024) Tailor-made molecular imprints for biological event intervention. *Trends Biotechnol.* 42, 1097–1111
9. Kunath, S. *et al.* (2015) Cell and tissue imaging with molecularly imprinted polymers as plastic antibody mimics. *Adv. Healthc. Mater.* 4, 1322–1326
10. León, C.H. *et al.* (2023) Synthetic peptide antibodies as TNF-α inhibitors: molecularly Imprinted polymer nanogels neutralize the inflammatory activity of TNF-α in THP-1 derived macrophages. *Angew. Chem.* 135, e202306274
11. Dong, Y. *et al.* (2019) Inhibition of HER2-positive breast cancer growth by blocking the HER2 signaling pathway with HER2-glycan-imprinted nanoparticles. *Angew. Chem. Int. Ed.* 58, 10621–10625
12. Cenci, L. *et al.* (2016) Guided folding takes a start from the molecular imprinting of structured epitopes. *Nanoscale* 8, 15665–15670
13. Gu, Z. *et al.* (2021) Molecularly imprinted polymer-based smart prodrug delivery system for specific targeting, prolonged retention, and tumor microenvironment-triggered release. *Angew. Chem. Int. Ed.* 60, 2663–2667
14. de Cássia Novaes, W. and Berg, A. (2003) Experiences with a new nonbiodegradable hydrogel (Aquamid): a pilot study. *Aesth. Plast. Surg.* 27, 376–380
15. Manafi, A. *et al.* (2010) Unacceptable results with an accepted soft tissue filler: polyacrylamide hydrogel. *Aesth. Plast. Surg.* 34, 413–422
16. Christensen, L.H. *et al.* (2003) Long-term effects of polyacrylamide hydrogel on human breast tissue. *Plast. Reconstr. Surg.* 111, 1883–1890
17. Amin, S.P. *et al.* (2004) Complications from injectable polyacrylamide gel, a new nonbiodegradable soft tissue filler. *Dermatologic Surg.* 30, 1507–1509
18. Caballero, D. *et al.* (2022) Precision biomaterials in cancer theranostics and modelling. *Biomaterials* 280, 121299
19. Goff, N.L. *et al.* (2020) Renewable plant oil-based molecularly imprinted polymers as biopesticide delivery systems. *ACS Sustain. Chem. Eng.* 8, 15927–15935
20. Suriyanarayanan, S. *et al.* (2023) Smart bio-nano interface derived from zein protein as receptors for biotinyl moiety. *Talanta* 256, 124298

21. Bossi, A.M. *et al.* (2021) Molecularly imprinted silk fibroin nanoparticles. *ACS Appl. Mater. Interfaces* 13, 31431–31439
22. Maniglio, D. *et al.* (2023) Silk fibroin molecularly imprinted nanoparticles as biocompatible molecular nanotraps: molecular recognition ties the knot with biomaterials. The bioMIP's labeling and degradation. *MRS Adv.* 8, 429–434
23. Gil, E.S. *et al.* (2005) Effect of β -sheet crystals on the thermal and rheological behavior of protein-based hydrogels derived from gelatin and silk fibroin. *Macromol. Biosci.* 5, 702–709
24. Shen, Y. *et al.* (2021) From protein building blocks to functional materials. *ACS Nano* 15, 5819–5837
25. Yue, K. *et al.* (2015) Synthesis, properties, and biomedical applications of gelatin methacryloyl (GelMA) hydrogels. *Biomaterials* 73, 254–271
26. Slaughter, B.V. *et al.* (2009) Hydrogels in regenerative medicine. *Adv. Mater.* 21, 3307–3329
27. Montazerian, H. *et al.* (2022) Bio-macromolecular design roadmap towards tough bioadhesives. *Chem. Soc. Rev.* 51, 9127–9173
28. Piao, Y. *et al.* (2021) Biomedical applications of gelatin methacryloyl hydrogels. *Eng. Regen.* 2, 47–56
29. Rachkov, A. and Minoura, N. (2000) Recognition of oxytocin and oxytocin-related peptides in aqueous media using a molecularly imprinted polymer synthesized by the epitope approach. *J. Chromatogr. A* 889, 111–118
30. Pasquardini, L. and Bossi, A.M. (2021) Molecularly imprinted polymers by epitope imprinting: a journey from molecular interactions to the available bioinformatics resources to scout for epitope templates. *Anal. Bioanal. Chem.* 413, 6101–6115
31. McGeer, P.L. and McGeer, E.G. (2004) Inflammation and the degenerative diseases of aging. *Ann. N. Y. Acad. Sci.* 1035, 104–116
32. Lan, T. *et al.* (2021) Inflammatory cytokines in cancer: comprehensive understanding and clinical progress in gene therapy. *Cells* 10, 100
33. Rea, I.M. *et al.* (2018) Age and age-related diseases: role of inflammation triggers and cytokines. *Front. Immunol.* 9, 586
34. Tanaka, T. *et al.* (2014) IL-6 in inflammation, immunity, and disease. *Cold Spring Harb. Perspect. Biol.* 6, a016295
35. Chen, L. *et al.* (2018) Inflammatory responses and inflammation-associated diseases in organs. *Oncotarget* 9, 7204
36. Hu, X. *et al.* (2021) The JAK/STAT signaling pathway: from bench to clinic. *Signal Transduct. Target. Ther.* 6, 1–33
37. Lima, A.C. *et al.* (2021) Modulating inflammation through the neutralization of Interleukin-6 and tumor necrosis factor-α by biofunctionalized nanoparticles. *J. Control. Release* 331, 491–502
38. Kang, S. *et al.* (2019) Targeting interleukin-6 signaling in clinic. *Immunity* 50, 1007–1023
39. Desmet, J. *et al.* (2014) Structural basis of IL-23 antagonism by an Alphabody protein scaffold. *Nat. Commun.* 5, 1–12
40. Lee, S.C. *et al.* (2012) Design of a binding scaffold based on variable lymphocyte receptors of jawless vertebrates by module engineering. *Proc. Natl. Acad. Sci. U. S. A.* 109, 3299–3304
41. Lee, J.J. *et al.* (2014) A high-affinity protein binder that blocks the IL-6/STAT3 signaling pathway effectively suppresses non-small cell lung cancer. *Mol. Ther.* 22, 1254–1265
42. Shi, C. *et al.* (2015) A drug-specific nanocarrier design for efficient anticancer therapy. *Nat. Commun.* 6, 7449
43. Shi, C. *et al.* (2020) A nanotrap improves survival in severe sepsis by attenuating hyperinflammation. *Nat. Commun.* 11, 3384
44. Myers, R.H. *et al.* (1989) Response surface methodology: 1966–l988. *Technometrics* 31, 137–157
45. Cenci, L. *et al.* (2018) Synthesis and characterization of peptide-imprinted nanogels of controllable size and affinity. *Eur. Polym. J.* 109, 453–459
46. Bucciarelli, A. *et al.* (2019) Preparation and statistical characterization of tunable porous sponge scaffolds using UV Cross-linking of methacrylate-modified silk fibroin. *ACS Biomater. Sci. Eng.* 5, 6374–6388
47. Li, Y. *et al.* (2023) Rational development of hypervalent glycan shield-binding nanoparticles with broad-spectrum inhibition against fatal viruses including SARS-CoV-2 variants. *Adv. Sci.* 10, 2202689
48. Suk, J.S. *et al.* (2016) PEGylation as a strategy for improving nanoparticle-based drug and gene delivery. *Adv. Drug Deliv. Rev.* 99, 28–51
49. Bossi, A.M. *et al.* (2012) Fingerprint-imprinted polymer: rational selection of peptide epitope templates for the determination of proteins by molecularly imprinted polymers. *Anal. Chem.* 84, 4036–4041
50. Slany, A. *et al.* (2016) Contribution of human fibroblasts and endothelial cells to the hallmarks of inflammation as determined by proteome profiling. *Mol. Cell. Proteomics* 15, 1982–1997
51. Rieckmann, J.C. *et al.* (2017) Social network architecture of human immune cells unveiled by quantitative proteomics. *Nat. Immunol.* 18, 583–593
52. Mier, A. *et al.* (2021) Molecularly imprinted polymer nanogels for protein recognition: direct proof of specific binding sites by solution STD and WaterLOGSY NMR spectroscopies. *Angew. Chem. Int. Ed.* 60, 20849–20857
53. Turkewitsch, P. *et al.* (1998) Fluorescent functional recognition sites through molecular imprinting. a polymer-based fluorescent chemosensor for aqueous cAMP. *Anal. Chem.* 70, 2020–2030
54. Chen, L. *et al.* (2016) Molecular imprinting: perspectives and applications. *Chem. Soc. Rev.* 45, 2137–2211
55. Chanput, W. *et al.* (2014) THP-1 cell line: an in vitro cell model for immune modulation approach. *Int. Immunopharmacol.* 23, 37–45
56. Schildberger, A. *et al.* (2013) Monocytes, peripheral blood mononuclear cells, and tHP-1 cells exhibit different cytokine expression patterns following stimulation with lipopolysaccharide. *Mediat. Inflamm.* 2013, 1–10
57. Liu, X. *et al.* (2018) LPS-induced proinflammatory cytokine expression in human airway epithelial cells and macrophages via NF-κB, STAT3 or AP-1 activation. *Mol. Med. Rep.* 17, 5484–5491
58. Anselmo, A.C. and Mitragotri, S. (2016) Nanoparticles in the clinic. *Bioeng. Transl. Med.* 1, 10–29
59. Zhong, L. *et al.* (2022) Molecularly imprinted polymers with enzymatic properties reduce cytokine release syndrome. *ACS Nano* 16, 3797–3807
60. Xu, S. *et al.* (2021) Molecularly imprinted polymer nanoparticles: an emerging versatile platform for cancer therapy. *Angew. Chem. Int. Ed.* 60, 3858–3869
61. Ren, T. *et al.* (2019) 3-D geometry and irregular connectivity dictate neuronal firing in frequency domain and synchronization. *Biomaterials* 197, 171–181
62. Vettorato, E. *et al.* (2024) Development and validation of novel Z-360-based macromolecules for the active targeting of CCK2-R. *Mol. Pharmacol.* 21, 3848–3865
63. Nečas, D. and Klapetek, P. (2012) Gwyddion: an open-source software for SPM data analysis. *Open Phys.* 10, 181–188
64. Harding, S.E. and Jumel, K. (1998) Light scattering. *Curr. Protoc. Protein Sci.* 11, 7.8.1–7.8.14
65. Park, E.K. *et al.* (2007) Optimized THP-1 differentiation is required for the detection of responses to weak stimuli. *Inflamm. Res.* 56, 45–50
66. Mozzini, C. *et al.* (2014) Increased endoplasmic reticulum stress and Nrf2 repression in peripheral blood mononuclear cells of patients with stable coronary artery disease. *Free Radic. Biol. Med.* 68, 178–185

STAR★METHODS

KEY RESOURCES TABLE

Reagent or resource	Source	Identifier
Chemicals, peptides, and recombinant proteins		
Gelatin type A	Sigma Aldrich	Cat#9000-70-8
Methacrylic anhydride	Sigma Aldrich	Cat#276685
Phosphate Buffer (PB)	Sigma Aldrich	Cat#P3619
Phosphate buffered saline (PBS)	Sigma Aldrich	Cat#P3813
Tris acetate	Sigma Aldrich	Cat#67996
Morpholino ethane sulfonic acid (MES)	Sigma Aldrich	Cat#M8250
Tris (hydroxymethyl)-aminomethane (Tris)	Sigma Aldrich	Cat#20-160
Lithium phenyl-2,4,6-trimethylbenzoylphosphinate (LAP)	Sigma Aldrich	Cat#900889
Poly(ethylene glycol) methacrylate (PEGMA)	Sigma Aldrich	Cat#409529
Nile Blue acrylamide	Sigma Aldrich	Cat#908673
Acryloxyethyl thiocarbamoyl rhodamine B	PolySciences	Cat#25404-100
Dimethyl Sulfoxide (DMSO)	Sigma Aldrich	Cat#20-139
Interleukin-6 C-terminal (IL-6Cterm) sequence: EFLQSSLRALRQM	OligoMaker ApS	https://oligomaker.com/
IL-6CtermTAMRA peptide	OligoMaker ApS	N/A
IL-6Cterm scramble of sequence: FLQERSSLRQMAL	OligoMaker ApS	N/A
Cardiac troponin I peptide of sequence: NIDALSGMEGR	OligoMaker ApS	N/A
Cardiac troponin I peptide of sequence: AYATEPHAK	OligoMaker ApS	N/A
Beta natriuretic peptide of sequence: EVATEGIR	OligoMaker ApS	N/A
Human serum albumin	Sigma Aldrich	Cat#A5843
Human serum transferrin	Sigma Aldrich	Cat#T8158
TNF-α	Sigma Aldrich	Cat#SRP3177
RPMI-1640 medium	Sigma Aldrich	Cat#R2405
Fetal Bovine Serum (FBS)	Sigma Aldrich	Cat#341506
Resazurin reagent	Chemodex	Cat#R0051
Triton X-100	Sigma Aldrich	Cat#T8787
Oregon green phalloidin	Molecular Probes	Cat#O7466
4',6-diamidino-2-phenylindole dilactate (DIPA)	Invitrogen	Cat#D3571
Critical commercial assays		
Chromogenic Limulus amebocyte lysate assay	Sigma Aldrich	Cat#E8029
AlamarBlue® assay	Thermo Fisher Scientific	Cat#DAL1025

(continued on next page)

(continued)

Reagent or resource	Source	Identifier
PE Annexin V Apoptosis Detection Kit	BD Bioscience	Cat#559763
7-amino-actinomycin D	BD Bioscience	Cat#559925
Simple Plex Cartridge Kit for IL-6; IL-8, TNF-alpha	BioTechne	Cat#SPCKC-PS-009470
Simple Plex Cartridge Kit for IL-6 Serum/Plasma	BioTechne	Cat#SPCKC-PS-009384
Experimental models: cell lines		
Macrophage-like THP-1	Clinisciences	Cat#C0003024
Software and algorithms		
R	Team, R.C. (2021) R Project. *R: A language and environment for statistical computing*.	https://www.r-project.org/
Gwyddion	Nečas, D. and Klapetek, P. (2012) Gwyddion: an open-source software for SPM data analysis. Open Physics 10, 181–188	https://gwyddion.net/
Zetasizer v.6.32	Malvern PanAnalytical	https://www.malvernpanalytical.com/en/support/product-support/zetasizer-range/zetasizer-advance-range/zetasizer-pro#software
Other		
LED ILH-XT01-S365-SC211-WIR200	Intelligent LED Solutions	Cat#301-81-178
SnakeSkin™ Dialysis Tubing	Thermo Fisher Scientific	Cat#88244
Zetasizer Nano ZEN3600	Malvern Instruments Ltd	https://www.malvernpanalytical.com/en
FP-8500 spectrofluorometer	Jasco	https://www.jasco.co.uk/index.html
96 Flat Bottom Black Polystyrene microtiter plates	ThermoScientific	Cat#437111
Solver Pro system	NT-MDT	https://www.ntmdt-si.com/
TALOS F200S	Thermo Scientific	https://www.thermofisher.com/order/catalog/product/TALOSF200S
Supra 40 FieldEmission Scanning Electron Microscopy	Zeiss	https://www.zeiss.com/microscopy/en/home.html
J-1500 spectropolarimeter	Jasco	https://www.jasco.co.uk/index.html
Infinite 200 Pro M Plex Microplate Reader – AV	Tecan	https://www.tecan.com/
FACSCanto II	BD Bioscience	https://www.bdbiosciences.com
Confocal microscope A1	Nikon	https://www.nikon.com
ELLA microfluidic immunoassay system	ProteinSimple, Bio-techne	https://www.bio-techne.com

EXPERIMENTAL MODEL AND STUDY PARTICIPANT DETAILS

Macrophage-like THP-1 cell line was obtained from Clinisciences.

METHOD DETAILS

GelMA preparation

Gelatin methacryloyl (GelMA) was prepared according to the protocol reported by Ren T. *et al.* [61] with slight modifications. A 10% w/V gelatin type A solution was prepared in PBS pre-heated at 50°C. The solution was left under stirring for 1 h and then 8 ml of methacrylic anhydride (8.28 g, 53.7 mmol) were added dropwise. The reaction solution was left under stirring at 50° for 2.5 h and then transferred into a 3.5 kDa MWCO dialysis bag and dialyzed against DI water at 40–45°C for 7–15 days until complete removal of unreacted species. The solution was then freeze-dried and lyophilized GelMA was stored at -20°C until use. The GelMA methacrylation yielded to a degree of functionalization equal to 70%, in line to what already reported by Vettorato E. *et al.* [62].

Synthesis of GelMA NPs

GelMA concentration was adjusted to 0.3% or 0.03% w/v in MilliQ water, or in the following buffers: 10 mM acetate Tris pH 3.5; 10 mM MES pH 5.0; 10 mM Tris HCl pH 7.0; 10 mM CAPSO pH 9.8. The solutions were heated at 80°C for 10 minutes, then at 50°C for 10 minutes and finally the temperature was set at 37°C. The photoinitiator lithium phenyl-2,4,6-trimethylbenzoylphosphinate (LAP) was added at the final concentration of 0.02% w/v, and photopolymerized for 1 minute under UV light λ=365 nm (radiant power 1.2 W). Samples were prepared at least in triplicate. Subsequent decorations were performed by the addition to the GelMA NPs synthetic batches of PEGMA (M_n 500 Da) in concentrations ranging from 0.5 to 500x mol:mol of GelMA NPs and by photopolymerization for 1 minute under UV light λ=365 nm. Decoration with fluorescent labels was performed by the addition of 40 µl of either acryloxyethyl thiocarbamoyl rhodamine B or Nile Blue acrylamide solutions dissolved at 0.02% in DMSO. At the completion of the syntheses, GelMA NPs were extensively dialyzed against water and PBS.

Synthesis of IL-6 GelMA nanotraps

GelMA concentration was adjusted to 0.3% in 5 mM of PB pH 7.0 buffer, in the presence of 6 nmol of the print molecule IL-6Cterm template peptide of sequence EFLQSSLRALRQM. The final volume was 2 ml. LAP was added at the final concentration of 0.05% w/v and polymerized as reported above. At the end of the polymerization process, the template was removed by the addition of Trizma free base to the NPs suspension to reach a pH of 10.5 for 1 hour. Samples were heated in the heating chamber at 45°C for 30 minutes under stirring to perform the thermal wash. Dialysis was performed in 300 ml of water for 1 hour and then in 3.5 l of water overnight under stirring, followed by further dialysis in 3.5 l of water for 3h repeated twice the following day. Samples were freeze-dried for storage. When used immediately, samples were dialyzed in PBS for 3 hours. Control nanotraps were prepared in the same manner but using a different template, i.e. peptide from the cardiac troponin I (cTnpI) of sequence NIDALSGMEGR.

Effect of the lyophilization on GelMA NPs

The effect of the lyophilization on the quality of GelMA NPs was studied by DLS. Lyophilized GelMA NPs were resuspended in 500 µl of PB 10 mM pH 7.4 for 3 hours. The hydrodynamic size and the PDI values of freshly synthesized GelMA NPs and reconstituted GelMA NPs were compared.

Effect of camouflage on the stability of the GelMA NPs

GelMA NPs and PEGMA-GelMA NPs were synthesized (3 mg/ml) and particle dimensions were next measured at DLS over time at 0, 4, 7, 11, 12, and 18 days. To verify the stability and the quality of GelMA NPs and camouflaged GelMA NPs were compared.

Effect of camouflage with PEGMA

GelMA NPs were entailed of PEGMA at concentrations 0x, 0.5x, 5x, 50x and 500x. Next the coupling to acryloxyethyl thiocarbamoyl rhodamine B was performed. Then, samples were extensively dialyzed and analyzed at DLS. Moreover, the emissions intensities of the fluorophores incorporated on GelMA NPs (1 and 2 µM) were measured on a Jasco FP-8500 spectrofluorometer using 1 cm path-length quartz cuvettes, excitation wavelength was 525 nm, emission wavelength was 575 nm. Moles of fluorophore incorporated were estimated by fluorescence calibration curves. The linear equation for Nile Blue acrylamide calibration curve was:

$$\text{Em intensity} = 2.4248 \text{ x } (\mu M) + 14.426 \quad [1]$$

while the linear equation for acryloxyethyl thiocarbamoyl rhodamine B calibration curve was:

$$\text{Em intensity} = 398.88 \text{x } (\mu M) + 12.908 \quad [2]$$

Response surface method

The entire statistical analysis was performed with the use of the programming language R following the statistical approach described in SI Section 3. An initial comparison by verifying the presence of significant differences among the different groups has been done by using the analysis of variance (ANOVA) followed by a Turkey multi-comparison test. The model goodness of fit was evaluated by the coefficient of determination (r2) and plotted as a matrix. The level of significance was assigned as follows $p \leq 0.1$ (.), $p \leq 0.05$ (*), $p \leq 0.01$ (**), $p \leq 0.001$ (***). Response Surface Methodology (RSM) was adopted to model the empirical equations to correlate the considered factors to the yields. In this case, we considered three continuous factors: the pH of the solution (4 levels, Factor A), the concentration of LAP photoinitiator (3 levels, Factor B), and the concentration of the GelMA (2 levels, Factor C). As yields, we considered the mean

dimension of the particles and the index of polydispersity. Trials are listed in Table S2.1. Equation 1 represents the complete model. An ANOVA test followed by a Turkey multi-comparison was conducted to verify the significance of each term of the reported equation. Only the terms with a significant effect ($p \leq 0.05$) were included in the model. F function, Equation 1, was chosen to normalize the model residues and to make them patternless. The whole model was considered significant with a p-value ≤0.05.

$$F(Y) = c_0 + c_1A + c_2B + c_3C + c_4AB + c_5AC + c_5BC + c_6ABC + c_7A^2 + c_8A^2B + c_9A^2C + c_{10}A^2BC + c_{11}A^3 + c_{12}A^3B + c_{13}A^3C + c_{14}A^3BC + c_{15}A^4 + c_{16}A^4B + c_{16}A^4C + c_{17}A^4BC$$

Atomic force microscopy (AFM)

Samples were imaged in semi-contact mode using super sharp diamond-like carbon tips (NSG01_DLC, NT-MDT, 1 nm nominal tip radius, 150 kHz, force constant 5.5 N/m), collecting 1 x 1 μm, 512 points resolution topography images. AFM data were analyzed with the support of Gwyddion analysis software [63].

Electron microscopy

SEM images were acquired in secondary electron mode at 5 kV, while TEM images were acquired with an acceleration voltage of 200 kV. GelMA nanotraps were suspended in a water solution at 1 mg/ml; the dispersion was further diluted 10, 100, and 1000 times in deionized MilliQ water. For FE-SEM, the dispersion was deposited onto a mono-crystalline gold-coated silicon chip (120 nm thickness) and freeze-dried to remove water, preserving the tridimensional structure, while for TEM, the dispersions were cast on a Formvar/Carbon Supported Copper Grids size 200 mesh and dried for imaging.

Dynamic light scattering (DLS)

Size distribution and polydispersity index (PDI) were determined by DLS using a Zetasizer Nano ZEN3600. GelMA nanotraps were dispersed in filtered deionized water at 0.3 mg/ml and filtered at 0.22 μm prior to measurement. The material refractive index (RI) was 1.490 and the absorption value 0.01; the dispersant RI was 1.332 for, the viscosity was 0.89 cP as reported by the Zetasizer v.6.32 software. The temperature was set at 310°K and a detection angle of 173° was used. Measurements were in triplicate.

Static light scattering (SLS)

A Zetasizer Nano ZEN3600 was used to measure the average molar mass (M_n) of the GelMA nanoparticles and GelMA nanotraps. Latex monosize standards 15-153 nm were used to calibrate the system. GelMA-NPs were diluted to reach concentrations in the range of 3-0.006 mg/ml and measured. Raw data were analyzed by the Debye plot, KC/Rθ versus particle concentration, where K is the optical constant, C is the particle concentration and Rθ is the sample Rayleigh ratio; the linear fit intercept corresponds to 1/Mn, following Harding, S.E. and Jumel, K. [64]. A particle refractive index increment (dn/dC) of 0.17 ml/g and a spherical particle shape (Rg = 0.740 Rh) were considered. The RI, viscosity, absorption values and the Rayleigh ratio were provided by the Zetasizer v.6.32 software, and the refractive index increment (dn/dC) was found in the American Polymer Standards Corporation.

Yield of the synthesis

The synthetic yield was calculated knowing the initial quantity of GelMA in each synthetic batch (triplicate). Each polymerized batch of GelMa nanotraps was dialyzed in water, freeze-dried and weighed. The results indicated the yield was > 90%.

Circular dichroism (CD)

CD measurements were carried out on a Jasco J-1500 spectropolarimeter equipped with a Peltier temperature-controlled cell holder. Far-UV spectra (190–250 nm) were recorded in 0.1 cm cuvettes at 25°C, with a scan rate of 20 nm min^{-1}, step resolution of 0.1 nm, a bandwidth of 1 nm, and an integration time of 2 s. Spectra were recorded on samples of GelMA NPs or of IL-6 nanotraps at the temperatures of 25, 37 and 50°C. Three spectra accumulations were averaged for each sample and the spectrum of the buffer was considered as a blank and subtracted. Spectra were recorded on samples of GelMA NPs or of IL-6 nanotraps at the temperatures of 25, 37 and 50 °C. Three spectra accumulations were averaged for each sample and the spectrum of the buffer was considered as a blank and subtracted.

Binding isotherm of IL-6 nanotraps

Nanotraps were resuspended in PBS 10 mM pH 7.4 at a final concentration of 2 mg/ml for 3 hours. A fixed quantity of 19 pmol/well of peptide IL-6Cterm-TAMRA in PBS 10 mM pH 7.4 was used to test the binding. Measurements were performed in triplicate on 96 Flat Bottom Black Polystyrene microtiter plates using a Tecan Infinite 200 Pro M Plex Microplate Reader – AV. Wells were loaded with a final volume of 100 ml, with increasing quantities (0.2–760 pmol/well) of IL-6 nanotraps, or control non-imprinted GelMA NPs, or nanotraps prepared with templates nonrelated to IL-6, i.e. the peptide of sequence NIDALGMEGR from the cardiac troponin I. Incubated for at least 30 minutes and read up to 360 minutes. The excitation was at the λ_{exc} = 522 nm, and emission was recorded in the range 528–640 nm. Maximum λem was 586 nm.

Competition experiments

Nanotraps were resuspended in PBS 10 mM pH 7.4 at a final concentration of 2 mg/ml. A fixed quantity of 9.5 pmol/well of peptide IL-6Cterm-TAMRA in PBS 10 mM pH 7.4 was used to test the binding. Measurements were performed in triplicate on 96 Flat Bottom Black Polystyrene microtiter plates using a Tecan Infinite 200 Pro M Plex Microplate Reader – AV. Wells loaded with a final volume of 200 ml. The fixed concentration of 2.5 pmol/well of IL-6 nanotraps was challenged with 1, 6, 44 and 76x moles of competitor IL-6Cterm (EFLQSSLRALRQM) or scrambled IL-6Cterm (FLQERSSLRQMAL); alternatively competition was with 0.13, 1.3, 13 and 26x moles of the competitor peptides nonrelated to IL-6 (i.e. peptides from the cardiac troponin I: NIDALSGMEGR; AYATEPHAK; peptide from the beta natriuretic peptide: EVATEGIR). After the incubation time (60, 120, 180 min), samples were read by λ_{exc} = 522 nm, and emission was recorded in the range 528-640 nm. Maximum λem was 586 nm. For protein competitions, the fixed concentration of 2.5 pmol/well of IL-6 nanotraps was challenged with 0.16, 1.6, 16x moles of the competitors: IL-6, human serum albumin, human serum transferrin, TNF–α, with respect to the IL-6Cterm-TAMRA.

Cell culture

Macrophage-like THP-1 cell line was cultured as previously described by Park, E.K. *et al.* [65]. Cells were maintained in RPMI-1640 medium supplemented with 10% fetal bovine serum (FBS). For differentiation to a macrophage phenotype, THP-1 cells were incubated with 10 ng/ml of phorbol myristate acetate (PMA) for 24h. Cells were then washed with serum-free RPMI-1640 medium prior to each experiment. Endotoxin contamination of cell cultures was routinely excluded with the chromogenic Limulus amebocyte lysate assay.

Cell proliferation and metabolism

THP-1 cell metabolism upon exposure to the nanotraps was evaluated through the AlamarBlue® assay. Cells (10^5/well; 5 replicates for each condition) were exposed to 20 µg of nanotraps for 3 and 8 days. At each time point, treated samples and controls were incubated with Resazurin reagent 10% in a complete medium at 37°C for 2 hours in a 96-well plate. After this time, 100 µl of the supernatant of each sample was transferred to a black 96-well plate. The fluorescence intensity at 535 nm was measured on a microplate reader using the absorbance at 590 nm as a reference and the complete medium and the AlamarBlue® reagent as negative controls.

Cell viability

Differentiated THP-1 cells ($5x10^5$ cells/well) were incubated with increasing concentrations (maximum 1.67 mg/ml) of IL-6 nanotraps in PBS 10 mM pH 7.4. Cellular viability was evaluated with PE Annexin V Apoptosis Detection Kit and 7-amino-actinomycin D (BD Bioscience, Franklin Lakes, NJ, USA) as previously reported by Mozzini, C. *et al.* [66] and analyzed by flow cytometry on FACSCanto II. The number of each type of cell was expressed as a percentage of the number of total stained cells.

Uptake of nanotraps by THP1 cells

About $5x10^5$ THP-1 cells were suspended in triplicate in a 24-multiwell plate and exposed to 10 ng/ml of phorbol myristate acetate (PMA) for 24h to induce macrophage differentiation for adhesion and microscopy inspection. A 100 µg of GelMA-PEG-Rhodamine-nanotraps were added overnight, then the adherent cells were fixed with 4% paraformaldehyde for 30 minutes, washed three times with PBS (15 minutes each time), and then were permeabilized using 0.1% Triton X-100 PBS solution for 30 min. After washing in PBS for 3 times (15 minutes each), cells were incubated with Oregon green phalloidin 5.0 µl/sample and DAPI (4',6-diamidino-2-phenylindole dilactate) 1.0 ml/well, 5.4 µl diluted in 25.0 ml PBS, for 45min at room temperature. After three rinses with PBS, samples were observed by confocal microscopy stimulating fluorescence emission from cell nuclei and cytoskeleton, together with the nanotrap's emission of Rhodamin B and Nile Blue (3^{rd} acquisition channel, red color).

Effect of nanotraps on the IL-6 levels in the cell inflammatory model

Differentiated THP-1 cells were stimulated with 1 µg/ml of LPS for 24 hours in the presence or in the absence of nanotraps (150 µg) in PBS 10 mM pH 7.4. After 24 hours the supernatants were collected and stored at -20°C. Alternatively, after 6 hours of LPS exposure, nanotraps (150 µg) were added to the cell culture for 1 hour, and the supernatants were then collected and stored at -20°C. Samples were at least in quadruplicate. IL-6, IL-8, TNF-α were measured in the supernatants by using specific Simple Plex assays run on the ELLA microfluidic immunoassay system, according to the manufacturer's instructions. The low limit of quantification was 0.28 pg/ml; the upper limit was 2652 pg/ml. Significant statistical variations were calculated by one-way ANOVA, followed by Tukey's Honest Significant Difference (HSD) test to assess the significance of differences between pairs of group means. The levels of significance for statistical differences are presented as $p < 0.05$(*), $p < 0.01$(**), and $p < 0.001$(***).

Dose–response relationship

Differentiated THP-1 cells were stimulated with 1 µg/ml of LPS for 24 hours in PBS 10 mM pH 7.4. After 24 hours the supernatants were collected and stored at -20°C. Supernatants were then used to perform dose-response experiments by the addition of nanotraps (respectively, 20, 100, and 200 µg) for 2 hours. Samples were performed in triplicate. IL-6 was measured as reported above. The correlation between the quantity of nanotraps on the level of IL-6 in the removed supernatants of differentiated THP-1 cells stimulated with LPS was assessed.